

# UNSUPERVISED DETECTION OF THIN WATER SURFACES IN SWOT IMAGES BASED ON SEGMENT DETECTION AND CONNECTION

*S. Lobry\*, F. Tupin*

LTCI, Télécom ParisTech  
Université Paris-Saclay  
75013, Paris, France

*R. Fjørtoft*

Centre National d'Etudes Spatiales  
31400, Toulouse, France

## ABSTRACT

The objective of the Surface Water and Ocean Topography (SWOT) mission is to regularly monitor the height of the earth's water surfaces. One of the challenges toward obtaining global measurements of these surfaces is to detect small water areas.

In this article we introduce a method for the detection of thin water surfaces, such as rivers, in SWOT images. It combines a low-level step (segment detection) with a high-level regularization of these features. The method is then tested on a simulated SWOT image.

**Index Terms**— SWOT, Classification, SAR, Linear features detection

## 1. INTRODUCTION

The SWOT mission aims at improving the spatiotemporal coverage of altimetry measurements both for oceans and continental water surfaces. This mission is jointly led by NASA's Jet Propulsion Laboratory (JPL) and the French space Agency, *Centre National d'Études Spatiales* (CNES). The main instrument of the SWOT mission is a Ka-band Radar Interferometer (KaRIn) which operates at 35.6 GHz (0.85cm) with an incidence angle from  $1^\circ$  to  $4^\circ$ . Using such a near-nadir incidence angle causes high variations in the pixel size (from 60 to 10m) in the range direction. Therefore, many continental water surfaces will appear as thin in SWOT images (especially in the near-nadir part of the image), in addition to rivers. One of the challenges faced in SWOT mission is the detection of thin water surfaces.

Detection of thin structures is a widely studied problem in image processing, as it leads to many applications. In [1], automatic road cracks detection is performed. It first selects pixels that are likely to belong to the crack network based on their intensities before connecting them. In [2], a morphological toolchain is used for the detection vessels in eye fundus images. Thin objects detection has also been studied for SAR

images in the framework of road detection, for mapping applications. In [3], a two-step approach is used; first a linear structure detection is performed, which are then connected using a high-level step. This method has been applied to water detection in [4] with the addition of a multiscale step. A morphological approach has also been applied in the framework of SWOT in [5]. In this paper, we use a two-step approach for the detection of thin elements in SWOT images. In a low-level step, candidate segments are selected based on a line detector. These segments are then connected using Dijkstra's algorithm [6] and connections are selected using a Markov Random Fields (MRF) process.

The proposed method is described in section 2. Results on SWOT simulated data are presented in section 3. Finally, we discuss the method in section 4.

## 2. METHOD

### 2.1. Overview

We illustrate the general workflow of the proposed method in Figure 1. The first step is a linear feature detection adapted to SAR images. We follow the work of [3] for this first step. The set of segments detected in the low-level step covers only parts of rivers, either because other parts are not straight lines or simply because the segment brightness is too low for it to be detected at the pixel level. Therefore a high-level step based on the segment detection is required.

First, pairs of candidate segments that could be consecutive in a river are selected, and a path-finding algorithm is performed to link them. A Markov Random Field (MRF) is then applied to the sets of connections in order to enforce basic geometrical properties of rivers, which yields a set of lines covering the rivers. Finally, a simple expansion step is performed in order to obtain a pixel-based detection of the rivers.

Compared to the work of [4], we have added new priors based on the geometrical shape of rivers. Furthermore, our method focuses only on narrow elements (as it is designed to be ran alongside a detector for large water bodies such as the one presented in [7]).

\*Thanks to CNES and "Futur & Ruptures" program for funding.

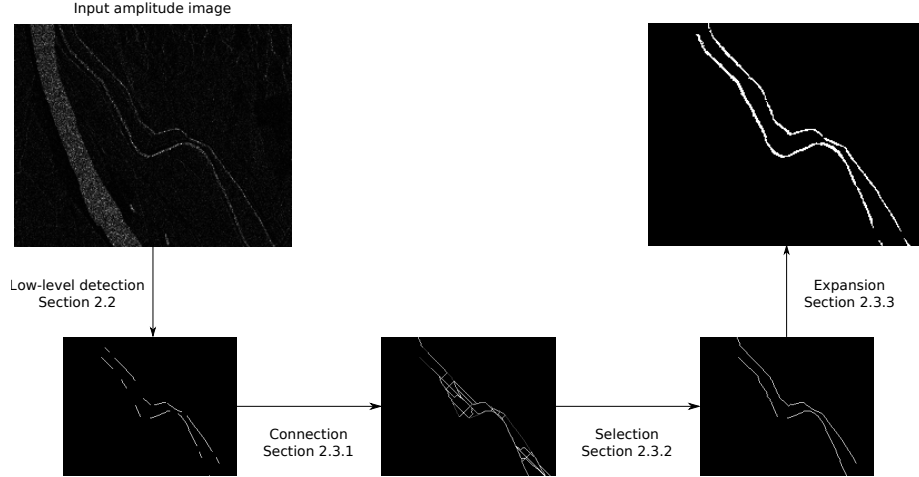


**Fig. 1:** Illustration of the different steps.

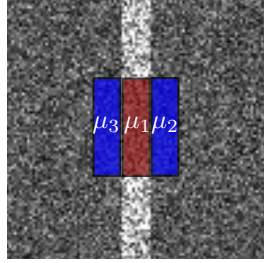


**Fig. 2:** Low-level line detector for vertical direction and fixed width

## 2.2. Low-level step

Segment detection in SAR images has been widely studied and we decided to use the same approach as in [3]. It models the segment as a rectangle  $\mu_1$  centered in a given pixel  $s$ , and compare it to the two surrounding segments ( $\mu_2$  and  $\mu_3$ , see Figure 2).

Two detectors are combined:

- D1: as we try to find bright segments, we compute the mean in amplitude of  $\mu_1$  and compare it to  $\mu_2$  and  $\mu_3$ .
- D2: computes the cross correlation between a mask and the regions.

These two detectors are applied for different widths (1 to 5 pixels) and different angles (16) then merged using an associative symmetrical sum:

$$l(i) = \frac{D1(i)D2(i)}{1 - D1(i) - D2(i) + 2D1(i)D2(i)}, \quad (1)$$

where  $l(i)$  indicates how likely a pixel  $i$  is a part of a segment. This image is then thresholded and detected pixels are

linearized allowing us to have a set of segments  $\mathcal{S}$  that are supposed to belong to rivers. Note that the thresholds used for this low-level step are chosen to give a very small false alarm rate.

## 2.3. Segment connection and regularization

### 2.3.1. Connection of segments

We use Dijkstra’s algorithm for the connection of candidate segments. As this algorithm can be computationally expensive (and depends on the space search for the connection), we restrict the connection to “compatible” segments. The compatibility between two segments is defined by the proximity of their extremities and the angular difference they form. For each compatible pair of segment  $(s_1, s_2)$  such that  $(s_1, s_2) \in \mathcal{S}^2$  and  $s_1 \neq s_2$ , we perform the classical Dijkstra’s algorithm.

We apply Dijkstra’s algorithm on a directed graph with nodes corresponding to the pixels of the image that are in the space search (a band starting and ending at the two extremities of the segments  $s_1$  and  $s_2$  to be connected), and edges which link to the 8 neighbors. Whereas a geodesic distance was defined in [8], the weight associated to an edge going to a node representing the pixel  $i$  is set to the opposite of the low-level step value of  $i$ :  $l(i)$ . By doing so, the “shortest path” will be the one going through pixels that are likely to belong to a segment. As we do not normalize the distance definition by the number of pixels in the path, long connections are penalized. The set of obtained connections after this step is named  $\mathcal{C}_D$ .

### 2.3.2. Selection of connections

While the union of  $\mathcal{S}$  and  $\mathcal{C}_D$  is likely to contains the rivers of the image,  $\mathcal{C}_D$  also contains many unwanted connections, as

it can be seen in Figure 1. To remove them, we use priors on the geometrical shape of a river:

- Rivers have few end points.
- Rivers have few intersections.
- Generally, an end point of a segment has only one connection.
- Connections should only fill gaps; therefore they should be short.
- Long segments strongly indicate the presence of rivers; they should be connected.

We enforce these priors in a Markov Random Field framework; we aim at selecting a set of connections from  $\mathcal{C}_D$ . Note that in [4], the authors also needed to label the whole set of segments:  $\mathcal{S} \cup \mathcal{C}_D$ . The problem is expressed as a labeling search: each connection  $co \in \mathcal{C}_D$ , is assigned a label  $x_{co}$  which is 1 for a connection labeled as a river and 0 otherwise. It yields the following energy minimization:

$$\hat{\mathbf{x}} = \arg \min_{\mathbf{x}} \sum_{co \in \mathcal{C}_D} U(l|x_{co}) + U_{\text{shape}}(\mathbf{x}), \quad (2)$$

where the likelihood term is  $U(l|x_{co} = 1) = \frac{1}{|co|} \sum_{i \in co} l(i)$  and  $U(l|x_{co} = 0) = 0$  and the prior  $U_{\text{shape}}(\mathbf{x})$  penalizes end points, intersections, forks, long connections and isolated long segments in the network. We denote by  $\mathcal{C}$  the set of connections of  $\mathcal{C}_D$  with  $\hat{x}_{co} = 1$ .

### 2.3.3. Expansion of segments and connections

The union  $\mathcal{N}$  of  $\mathcal{S}$  and  $\mathcal{C}$  indicates the presence of rivers as chains of pixels with a width of 1 pixel. To recover a pixel-based classification and improve the positioning of the rivers, a local classification is needed. A direct classification as in [7] is not possible due to the thinness of the rivers and the noise level. Therefore, a local denoising approach is first applied. NL-SAR algorithm [9] has been chosen due to its good preservation of edges and lines. Since it is based on patch matching, it follows locally the river to compute the denoised values. We apply NL-SAR to the bounding box of each connected component extracted from  $\mathcal{N}$  (Figure 3(b)). The denoised image is then thresholded based on the theoretical intensity of the water in SWOT images in order to have a binary map of water (Figure 3(c)). A labeling in connected components is then performed and the component which has the largest intersection with the connected component from  $\mathcal{N}$  is selected.

## 3. RESULTS

The SWOT image used for the evaluation of the proposed method is a simulation based on a Digital Elevation Model (DEM) and landcover map of the Camargue area, France [10]

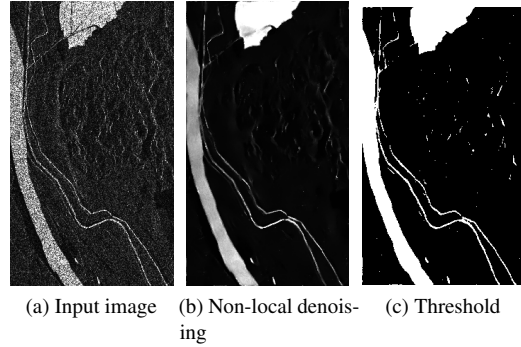


**Fig. 3:** Segment expansion

|     | Camargue |              |
|-----|----------|--------------|
|     | [7]      | [7] + Rivers |
| TPR | 92.98%   | 93.26%       |
| FPR | 1.12%    | 1.17%        |
| MCC | 0.9236   | 0.9240       |
| ER  | 12.71%   | 12.66%       |

**Table 1:** Classification results for the Camargue area

shown in Figure 4(a). The azimuth resolution is 10m and the range resolution goes from 60 to 10m. The image size is  $1839 \times 2979$  pixels. We show visual results in Figure 4. Note that we have many false negatives in the result for the detected rivers, as we only aim at finding narrow elements (and test the result against the whole ground truth). As this method is designed to be run alongside a classification algorithm for larger water surfaces, we provide results combined with the method proposed in [7] in Figure 4(c).

In the framework of the SWOT mission, the metric used for the evaluation of the algorithms is the Error Rate (ER, lower is better) defined as:

$$\text{ER} = \frac{FP + FN}{TP + FN}. \quad (3)$$

We also use the the Matthews correlation coefficient (MCC, higher is better) defined as:

$$\text{MCC} = \frac{TP \times TN - FP \times FN}{\sqrt{(TP + FP)(TP + FN)(TN + FP)(TN + FN)}}, \quad (4)$$

Numerical results are give in Table 1. We can see that we have a small improvement due to the addition of the proposed method.

## 4. CONCLUSION

The proposed method combines an object detection low-level step and a high-level step connecting the linear features for the detection of narrow water bodies in SWOT images. We

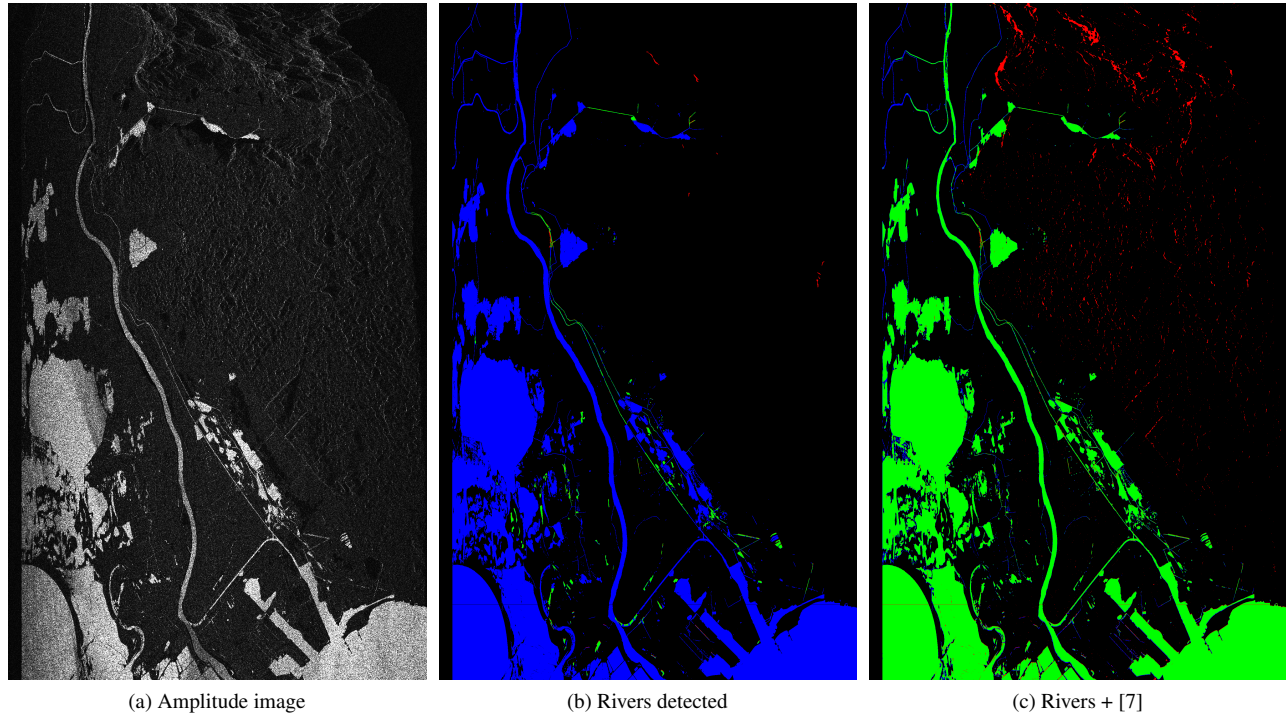


**Fig. 4:** Results on the Camargue dataset. Green, black, blue and red are for true positive, true negative, false negative and false positive respectively

show some preliminary results on a simulated SWOT image demonstrating the effectiveness of the method.

Further works include extensive tests on a wide range of images and a simplification of the processing chain for operational purposes.

## 5. REFERENCES

- [1] R. Amhaz, S. Chambon, J. Idier, and V. Baltazart, "Automatic crack detection on two-dimensional pavement images: An algorithm based on minimal path selection," *IEEE Transactions on Intelligent Transportation Systems*, vol. 17, no. 10, pp. 2718–2729, Oct 2016.
- [2] F. Rossant et al., "A morphological approach for vessel segmentation in eye fundus images, with quantitative evaluation," *Journal of Medical Imaging and Health Informatics*, vol. 1, no. 1, pp. 42–49, 2011.
- [3] F. Tupin et al., "Detection of linear features in SAR images: application to road network extraction," *Geoscience and Remote Sensing, IEEE Transactions on*, vol. 36, no. 2, pp. 434–453, 1998.
- [4] F. Cao et al., "Extraction of water surfaces in simulated Ka-band SAR images of KaRIn on SWOT," in *Geoscience and Remote Sensing Symposium (IGARSS), 2011 IEEE International*. IEEE, 2011, pp. 3562–3565.
- [5] S. Grosdidier et al., "River network detection on simulated SWOT images based on curvilinear denoising and morphological detection," in *2012 IEEE International Geoscience and Remote Sensing Symposium*, July 2012, pp. 5454–5457.
- [6] E.-W. Dijkstra, "A note on two problems in connexion with graphs," *Numerische mathematik*, vol. 1, no. 1, pp. 269–271, 1959.
- [7] S. Lobry et al., "Water segmentation in SAR images by joint detection and reflectivity estimation," in *Geoscience and Remote Sensing Symposium (IGARSS), 2017 IEEE International*. IEEE, 2017 (submitted).
- [8] T. Perciano et al., "A two-level Markov random field for road network extraction and its application with optical, SAR, and multitemporal data," *International Journal of Remote Sensing*, vol. 37, no. 16, pp. 3584–3610, 2016.
- [9] C.-A. Deledalle et al., "NL-SAR: A unified nonlocal framework for resolution-preserving (Pol)(In)SAR denoising," *Geoscience and Remote Sensing, IEEE Transactions on*, vol. 53, no. 4, pp. 2021–2038, April 2015.
- [10] J. Duro et al., "Simulation of near-nadir bistatic high resolution InSAR data in Ka-band for the SWOT mission," in *EUSAR 2014; 10th European Conference on Synthetic Aperture Radar*, June 2014, pp. 1–4.